

Article

The Paleoproterozoic Kandalaksha-Kolvitsa Gabbro-Anorthosite Complex (Fennoscandian Shield): New U–Pb, Sm–Nd, and Nd–Sr (ID-TIMS) Isotope Data on the Age of Formation, Metamorphism, and Geochemical Features of Zircon (LA-ICP-MS)

Ekaterina N. Steshenko *, Tamara B. Bayanova and Pavel A. Serov 

Geological Institute—Subdivision of the Federal Research Centre, Kola Science Centre of the Russian Academy of Sciences, Fersman St. 14, 184209 Apatity, Russia; tamara@geoksc.apatity.ru (T.B.B.); serov@geoksc.apatity.ru (P.A.S.)

* Correspondence: steshenko@geoksc.apatity.ru

Received: 20 January 2020; Accepted: 6 March 2020; Published: 10 March 2020



Abstract: The paper provides new U–Pb, Sm–Nd, and Nd–Sr isotope-geochronological data on rocks of the Paleoproterozoic Kandalaksha-Kolvitsa gabbro-anorthosite complex. Rare earth element (REE) contents in zircons from basic rock varieties of the Kandalaksha-Kolvitsa area were analyzed in situ using laser ablation inductively coupled plasma mass spectrometry (LA-ICP-MS). Plots of REE distribution were constructed, confirming the magmatic origin of zircon. Temperatures of zircon crystallization were estimated using a Ti-in-zircon geochronometer. The U–Pb method with a ^{205}Pb artificial tracer was first applied to date single zircon grains (2448 ± 5 Ma) from metagabbro of the Kolvitsa massif. The U–Pb analysis of zircon from anorthosites of the Kandalaksha massif dated the early stage of the granulite metamorphism at 2230 ± 10 Ma. The Sm–Nd isotope age was estimated on metamorphic minerals (apatite, garnet, sulfides) and whole rock at 1985 ± 17 Ma (granulite metamorphism) for the Kolvitsa massif and at 1887 ± 37 Ma (high-temperature metasomatic transformations) and 1692 ± 71 Ma (regional fluid reworking) for the Kandalaksha massif. The Sm–Nd model age of metagabbro was 3.3 Ga with a negative value of $\epsilon\text{Nd} = 4.6$, which corresponds with either processes of crustal contamination or primary enriched mantle reservoir of primary magmas.

Keywords: anorthosite; single zircon grains; U–Pb; Sm–Nd; Nd–Sr; ϵNd ; Ti-in-zircon

1. Introduction

Gabbro-anorthosite complexes occur in almost every ancient Hadean craton in the world (Pilbara and Yilgarn in Australia, Fiskenaeset in Greenland, Karnataka in India, etc.) [1–3]. In the Baltic Shield, gabbro-anorthosite magmatism is widespread from the Mesoproterozoic to the Paleoproterozoic (Figure 1) and associated with the formation of strategic mineral deposits (Cu–Ni, Ti–V, Pt–Pd, etc.) [4]. The Kolvitsa gabbro-anorthosite massif is located in the south of the Kola Peninsula, in the Kolvitsa Guba area of the Kandalaksha Bay of the White Sea.

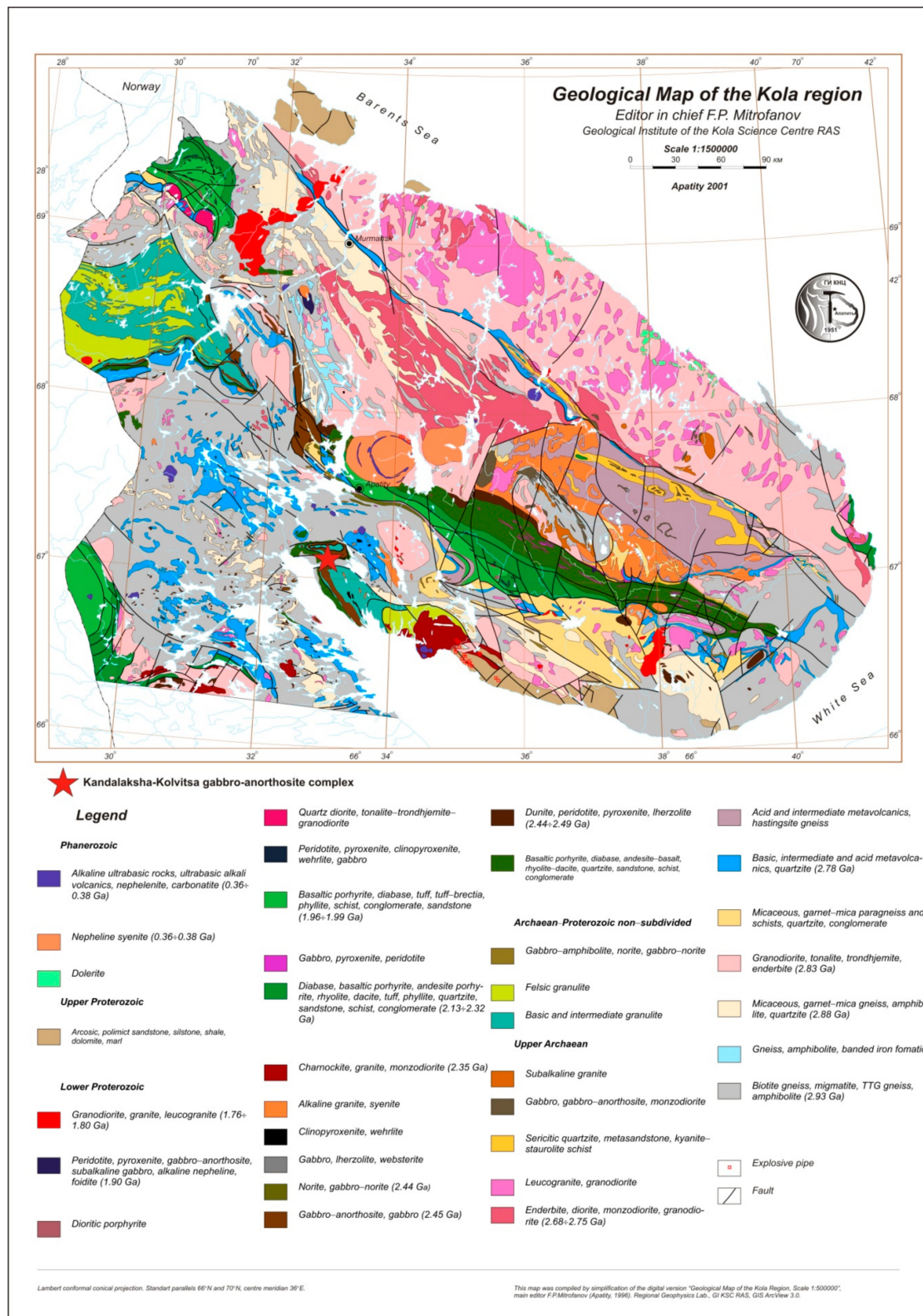


Figure 1. Geological map of the Kola region [5].

The Kandalaksha-Kolvitsa area is located in the southern part of the Lapland Granulite Belt (LGB) and comprises volcanogenic sequences intercalated by bodies of anorthosites. The Kandalaksha-Kolvitsa gabbro-anorthosite area tends to attract much attention for isotope-geochemical research as an object promising for platinum group elements (PGE) ores. It is suggested to

have a magmatic (plume?) origin, since rocks of the Kandalaksha-Kolvitsa zone have similar isotope-geochronological features with layered PGE intrusions in the Baltic Shield (Fedorovo-Pana massif, Monchetundra massif, etc.) [6]. This paper focused on the dating of the formation and the further metamorphic reworking of the Kandalaksha and Kolvitsa anorthosite massifs. U–Pb analysis on a single grain and Sm–Nd dating on rocks and minerals were provided for these purposes. The age of the Kolvitsa massif was estimated at 2450 ± 7 Ma [7] and 2462 ± 7 Ma [8]. Several stages of metamorphism were identified in the Kandalaksha-Kolvitsa area [9].

2. Geological Setting

The geological structure of the northwestern part of the Kolvitsa gabbro-anorthosite massif was studied during field work in 2012 (Figure 2). The bottom part of the massif hosts the Kandalaksha sequence of meso-melanocratic garnet amphibolites, with a thickness of 200 m to 2.0 km. The age of the sequence was estimated by the U–Pb method on a single zircon grain at 2467 ± 3 Ma [10]. Up the section, the Kolvitsa massif of gabbro-anorthosites stretches for at least 20 km. Its section is represented by 20-km-thick leucocratic metagabbro in the bottom part. The 1–2-km-thick middle part is composed of metaanorthosites, which are sporadically intercalated by thin layers and lenses of leucogabbro. The upper part (200-m to 1.5-km-thick) is represented by metagabbro. The massif is overlain by the Ploskaya Tundra suite of garnet-pyroxene-plagioclase crystalline schists as thick as at least 2 km (Figure 2).

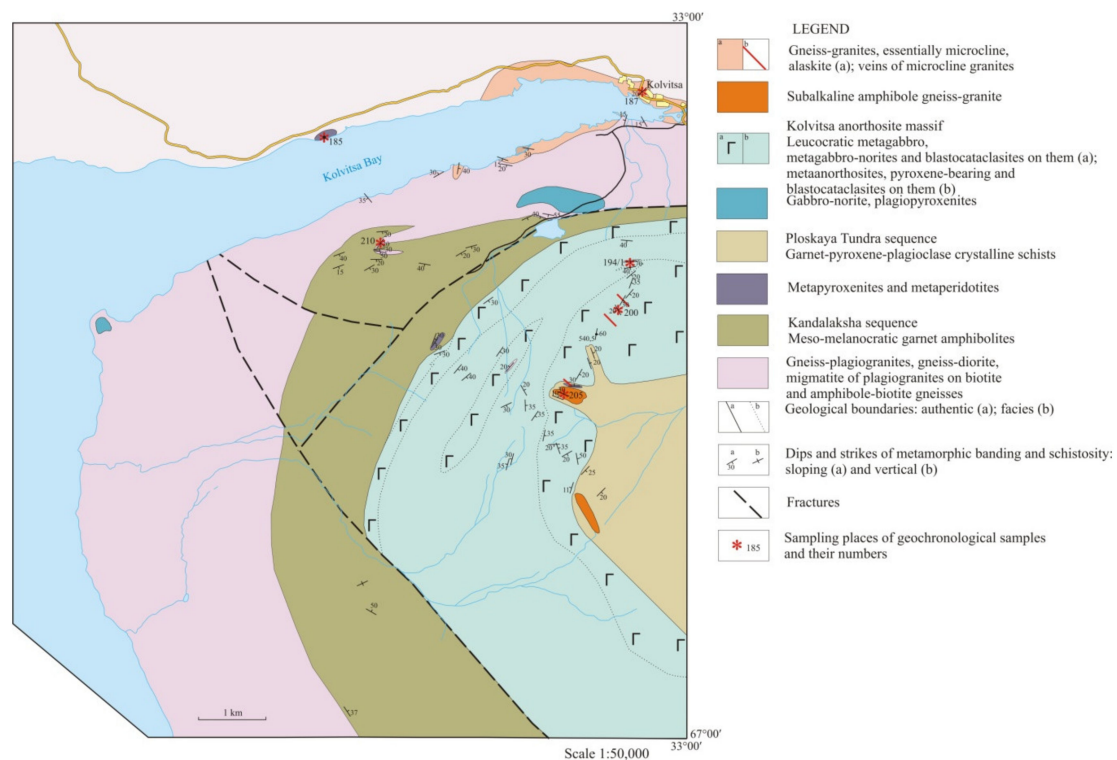


Figure 2. Scheme of the geological structure of the northwestern part of the Kolvitsa anorthosite massif.

The Kandalaksha gabbro-anorthosite massif consists of two flanks with a centroclinal closure in the west, mostly with a counter dip of banding and schistosity under the angles of $15\text{--}60^\circ$. It indicates a trough-like shape of the massif in section. The massif occurs on garnet amphibolites of the Kandalaksha sequence and is overlapped by garnet-pyroxene-plagioclase crystal schists of the Ploskaya Tundra sequence, which are similar to the rocks of the Kolvitsa massif (Figure 3). The basement of the Kandalaksha massif comprises a part of the marginal zone with a visible thickness of a few meters. This part consists of mesocratic metanorites. The major area of the intrusion is differentiated, like the

Kolvitsa massif. The main part of the massif in the bottom part is represented by a 200–300-m-thick discontinuous band of leucocratic metagabbro. Up the section, they are replaced by a zone of alternating metaanorthosites and leucocratic metagabbro with the thickness of 200–300 m to 1 km each (Figure 3). As a result, finely banded blastomylonites and blastocataclasites composed of garnet-plagioclase, garnet-pyroxene-plagioclase, and garnet-amphibole-plagioclase crystal schists were deformed.

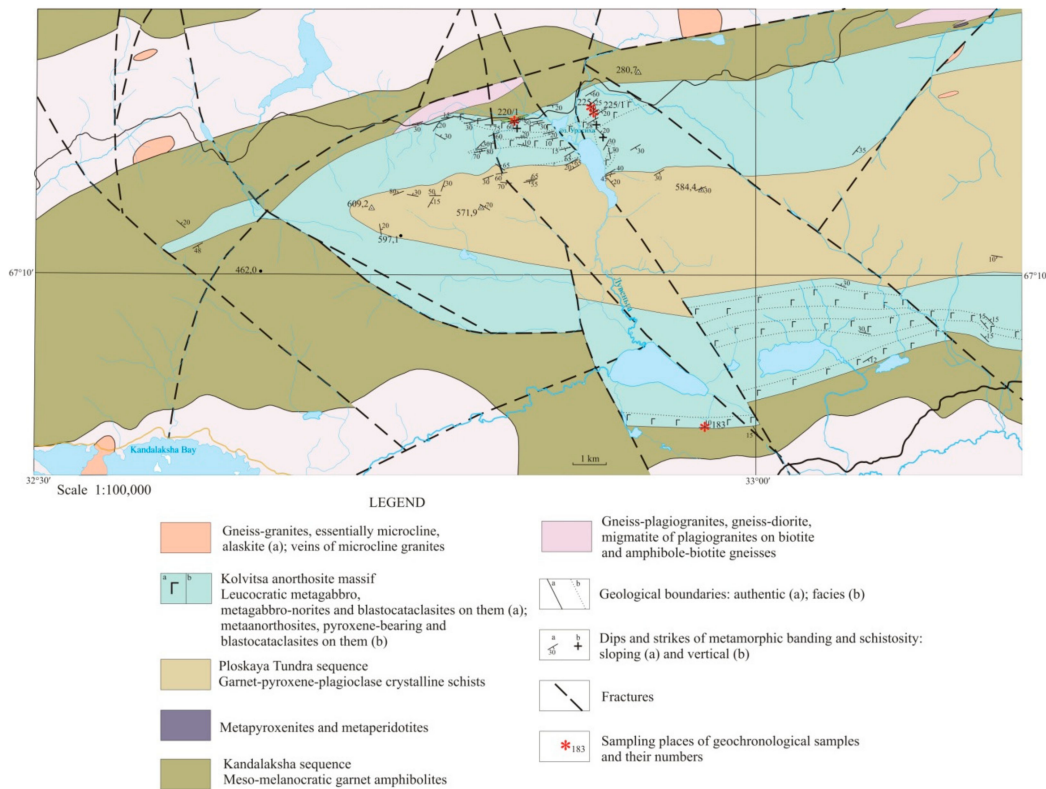


Figure 3. Scheme of the geological structure of the western part of the Kandalaksha anorthosite massif.

3. Materials and Methods

3.1. LA-ICP-MS

Trace and rare earth elements (REE) analyses of zircon crystals were carried out in situ on polished thin sections by laser ablation inductively coupled plasma mass spectrometry (LA-ICP-MS) using a Perkin Elmer ELAN 9000 DRC-e quadrupole mass spectrometer equipped with a 266-nm UP-266 MACRO laser (New Wave Research) following the technique described by the authors of [11] at the Tananaev Institute of Chemistry KSC RAS (Apatity, Russia).

Experiments were carried out using argon with a repetition rate of 10 Hz, pulse duration of 4 ns, and an energy density of 14–15 J/cm² at a spot with a diameter of 35–100 μm. External calibration was carried out using NIST 612 glass with the known contents of REE, U, and Th of 40 ppm as a multipoint calibration forced through the origin after blank correction. The diameter of the laser beam was changed, while all of the rest parameters remained the same: From 35 μm to 240 μm ($r = 0.999$) [11–13]. Sample NIST SRM 610 with the content of 450 ppm was used to check the accuracy of data reduction [14–16]. Considering calibration standards, measurements of the elements were within the range of 15% relative deviations. The precision was commonly 15% relative standard deviation (RSD) for all isotopes after the internal correction of the diameter of the laser beam. The determination limits were in the range of 0.01 ppm when the diameter of the laser beam was 155 μm, which was in compliance with the available data [17–19]. The results were verified in interlaboratory cross-checks and analyses of internationally approved standard zircon samples 91500, TEMORA 1, and Mud Tank [11–13].

3.2. U–Pb Dating

The method proposed by Krogh [20] was used to dissolve samples in strong (48%) hydrofluoric acid at the temperature of 205–210 °C over 1–10 days. In order to dissolve fluorides, the samples were reacted with 3.1 N HCl at the temperature of 130 °C for 8–10 h. To determine the isotope composition of Pb and concentrations of Pb and U, a sample was divided into two aliquots in 3.1 N HCl, then a mixed $^{208}\text{Pb}/^{235}\text{U}$ tracer was added. Pb and U were separated on an AG 1 × 8, 200–400 mesh anion exchanger in Teflon columns. A laboratory blank for the whole analysis was <0.1–0.08 ng for Pb and 0.01–0.04 ng for U. All isotope determinations were made on Finnigan MAT-262 mass spectrometers (Geological Institute KSC RAS, Apatity, Russia). The Pb isotope composition was analyzed on a secondary ion multiplier on a Finnigan MAT-262 in an ion-counting mode. Measurements of the Pb isotope composition are accurate to 0.025% when calibrated against NBS SRM-981 and SRM-982 standards. U and Pb concentrations were measured in a single filament mode with H_3PO_4 and silica gel added. The method described by the authors of [21,22] was used. Pb and U concentrations were measured in temperature ranges of 1350–1450 °C and 1450–1550 °C, respectively. Isotope ratios were corrected for mass discrimination during static processing of replicate analyses of the SRM-981 and SRM-982 standards ($0.12 \pm 0.04\%$ per a.m.u. for the Finnigan MAT-262). Errors in the U–Pb ratios were calculated during the statistical treatment of replicate analyses of the IGF-87 standard. They were assumed equal to 0.5% for Finnigan MAT-262. Isochrons and sample points were calculated using the Squid and Isoplot programs [23,24]. Age values were calculated with the conventional decay constants for U [25]. All errors are reported for a 2-sigma level. Corrections for common Pb were made as described by the authors of [26]. Corrections were also made for the composition of Pb separated from syngenetic plagioclase or microcline if the admixture of common Pb was >10% of the overall Pb concentration and the $^{206}\text{Pb}/^{204}\text{Pb}$ ratios were <1000.

3.3. Sm–Nd Dating

The isotope research was carried out in the Collective Use Centre of the Kola Science Centre RAS (Apatity, Russia). First, the samples were prepared by crushing, then minerals were separated using heavy liquids and mineral fractions were selected under binocular microscope.

In order to define concentrations of Sm and Nd, the sample was mixed with a compound tracer $^{149}\text{Sm}/^{150}\text{Nd}$ prior to dissolution. It was then diluted with a mixture of HF + HNO_3 (or + HClO_4) in Teflon sample bottles at a temperature of 100 °C until complete dissolution. Further extraction of Sm and Nd was carried out using standard procedures with two-stage ion-exchange and extraction-chromatographic separation using ion-exchange tar “Dowex” 50 × 8 in chromatographic columns employing 2.3 N and 4.5 N of HCl as an eluent. The separated Sm and Nd fractions were transferred into a nitrate form, upon which the samples (preparations) were ready for mass-spectrometric analysis.

The isotope Nd composition and Sm and Nd contents were measured using a seven-channel solid-phase mass-spectrometer Finnigan-MAT 262 (RPQ) in a static double-band mode, using Ta + Re filaments. The mean value of the $^{143}\text{Nd}/^{144}\text{Nd}$ ratio in a JNdi-1 standard was 0.512081 ± 13 ($N = 11$) in the test period. The error in $^{147}\text{Sm}/^{144}\text{Nd}$ ratios was 0.3% (2σ), which is a mean value for seven measurements in a BCR-2 standard [27]. An error in estimation of isotope Nd composition in an individual analysis was up to 0.01% for minerals with low Sm and Nd contents. The blank intralaboratory contamination was 0.3 ng in Nd and 0.06 ng in Sm. The accuracy of estimation of Sm and Nd contents was $\pm 0.5\%$. Isotope ratios were normalized per $^{146}\text{Nd}/^{144}\text{Nd} = 0.7219$, and then recalculated for $^{143}\text{Nd}/^{144}\text{Nd}$ in JNdi-1 = 0.512115 [28]. Parameters of isochrons were estimated using the ISOPLOT program complex [29]. Values of $\epsilon\text{Nd}(T)$ and T(DM) model ages were estimated using present-day values of CHUR as described by the authors of [30] at ($^{143}\text{Nd}/^{144}\text{Nd} = 0.512630$, $^{147}\text{Sm}/^{144}\text{Nd} = 0.1960$) and DM as described by the authors of [31] ($^{143}\text{Nd}/^{144}\text{Nd} = 0.513151$, $^{147}\text{Sm}/^{144}\text{Nd} = 0.2136$).

3.4. Rb-Sr Method for Whole-Rock Samples

Distilled acids HCl, HF, HNO₃, and H₂O (distillate) were used to decompose samples and minerals. Minerals of the analyzed samples (20–100 mg, depending on the amount of Rb and Sr, 200 mg of a rock) were decomposed in 4 mL of mixed HF and HNO₃ (proportion 5:1) in closed Teflon boxes in a thermostat at ~200 °C for about a day. Then, the produced solution was divided into two aliquots to estimate the isotope composition and contents of Rb and Sr. The latter were estimated by isotope dissolution using a ⁸⁵Rb/⁸⁴Sr mixed tracer. Rb and Sr were extracted by the elution chromatography on Dowex resin 50 × 8 (200–400 mesh) and 1.5 N and 2.3 N of HCl were used as eluates. The amount of resin in the used columns is ~7 cm³ and ~4 cm³. Extracted Rb and Sr concentrates were evaporated dry and then treated with several drops of HNO₃. The isotope composition of Sr and contents of Rb and Sr was estimated on MI-1201-T mass spectrometer in a double-band mode using Ta + Re filaments (Collective Use Centre of the Kola Science Centre RAS (Apatity, Russia)). Prepared samples were placed onto the bands in a nitric form. The isotope composition of Sr in all of the measured samples was normalized per 0.710248 [32]. Errors in estimations of the Sr isotope composition (95% confidence interval) were not higher than 0.04%; errors in estimations of Rb-Sr ratios were 1.5%. The blank intralaboratory contamination in Rb and Sr was 2.5 ng and 1.2 ng, respectively. Correction of mass fractionation for Sr isotopic ratios was based on an ⁸⁸Sr/⁸⁶Sr value of 8.37521 using a power law.

4. Results

4.1. Rock Samples and Minerals

Representative geochronological, geochemical, and petrographical samples were collected from major rock varieties of the Kandalaksha-Kolvitsa complex for further complex isotope-geochemical and geochronological research.

Two zircon morphotypes were separated from metagabbro of the Kolvitsa massif (sample 200) to study REE distribution in zircon and to provide precise U–Pb dating. The first variety of zircon was represented by isometric water-transparent crystals with noncorroded surfaces. The average grain size was 0.105 mm × 0.105 mm and the elongation coefficient was 1. The intraphase heterogeneity was poorly observed in back scattered electrons (BSE) and cathodoluminescence light (CL). The second morphotype was represented by prismatic light brown semi-transparent crystals with weakly corroded surfaces. The average size of crystals was 0.175 mm × 0.105 mm and the elongation coefficient was 1.6. The intraphase heterogeneity was detected in BSE and CL. It was represented by a fine rhythmic zoning. Besides, heavy concentrations of apatite, garnet, and sulfide minerals were separated from metagabbro (sample 200) for Sm–Nd isotope-geochemical and geochronological research.

A representative geochronological sample (183) of metagabbro was collected during field works in the Kandalaksha anorthosite massif to estimate the U–Pb age of its rocks and to study the REE distribution in zircon. Three types of zircon were extracted from this sample. The first type of zircon was represented by prismatic, semi-transparent, light yellow, weakly corroded crystals with an elongation coefficient of 2.5 (0.175 mm × 0.07 mm). The intraphase heterogeneity was detected in BSE and CL. It was represented by a fine rhythmic zoning. The second type of zircon was characterized by prismatic semi-transparent crystals and their zircon-type fragments with light yellow color, glossy luster and weakly corroded surfaces, and the elongation coefficient of grains was 1.6 (0.175 mm × 0.105 mm). BSE and CL studies indicated the intraphase heterogeneity. The third type of zircon was represented by milky white crystal fragments with an elongation coefficient of 1.0 (0.140 mm × 0.140 mm) and the intraphase heterogeneity, as indicated by BSE studies. Besides, heavy concentrations of apatite, amphibole, and garnet were separated from metagabbro (sample 183) for Sm–Nd isotope-geochemical and geochronological research.

Two zircon morphotypes (sample 225/1) were separated from anorthosites of the Kandalaksha massif for geochronological, isotope-geochemical, and mineralogical studies (U–Pb, REE distribution in zircon). Grains of two types were sampled for the U–Pb dating from a monomineral concentrate

of zircons (sample 225/1, Kandalaksha massif). The first type was represented by transparent pink fragments of zircon with sizes of up to 250 μm (content of U—13.5 ppm, Pb—12.5 ppm). The second type was represented by dark pink fragments of zircons with a yellow hue.

Monomineral concentrates of rutile, garnet, plagioclase, and clinopyroxene were sampled from metaorthosites of the Kandalaksha massif (sample 225/1) for the Sm–Nd studies.

4.2. Trace Element Geochemistry of Zircon

Five zircon grains of four morphotypes with low total REE contents (38.8 ppm to 918.4 ppm) were studied (Table 1). The spectra of REE distribution in zircon crystals were characterized by a minor amount of light REE and major amounts of heavy REE. It displayed a steep positive slope with negative Eu-anomalies and positive Ce-anomalies, which confirmed the magmatic origin of these grains (Figure 4).

Table 1. REE, Hf, and Ti contents in zircon from metagabbro of the Kolvitsa massif.

Elements	Sample Numbers *				
	8-1-1	8-1-2	8-2-2	8-3-2	8-4-2
	Contents, ppm				
Y	46.5	95.2	160.8	1095	126.9
La	0.01	0.04	0.01	0.14	0.01
Ce	0.16	0.30	2.36	12.1	1.30
Pr	0.01	0.01	0.02	0.01	0.01
Nd	0.88	1.22	0.77	2.66	1.43
Sm	1.60	0.74	1.01	2.66	0.41
Eu	0.15	0.15	0.10	0.43	0.01
Gd	2.10	1.77	3.41	9.30	6.68
Tb	0.58	0.54	0.91	2.92	1.97
Dy	5.19	8.62	13.6	44.6	13.0
Ho	2.30	3.13	4.67	23.4	4.29
Er	7.50	15.8	20.4	150.4	19.8
Tm	1.93	4.12	6.33	44.1	3.18
Yb	13.3	40.1	50.5	503.8	33.4
Lu	3.05	7.37	7.32	121.8	4.33
Total REE	38.8	84.0	111.4	918.4	89.8

Sample Number	Contents, Ti, ppm	Temperature, °C	T _{aver.} °C
8-1-1	10.6	746.5	
8-1-2	27.1	837.0	
8-3-2-1	22.1	815.6	
8-3-2-2	11.7	754.9	778
8-4-2-1	21.3	812.1	
8-4-2-2	8.12	723.2	

Note: * average amounts of REE in a crystal.

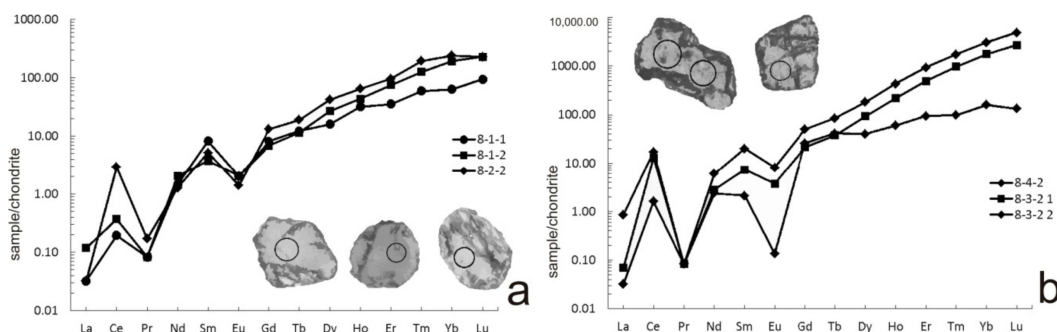


Figure 4. REE pattern in zircon crystals from metagabbro of the Kolvitsa massif (sample 200), normalized after Reference [33]. (a) Samples 8-1-1, 8-1-2 and 8-2-2; (b) Samples 8-3-2 and 8-4-2.

Notably, the amount of light REE was minor, which explains the low values of $(La/Yb)_N = 2.783\text{--}7.519$. Zircons are rich in Ce. The $(Ce/Ce^*)_N$ ranged from 0.0016 to 0.1249 and was poor in Eu, while the $(Eu/Eu^*)_N$ was 0.0079–0.0719 [34].

The technique described by the authors of [11] was applied to study REE in zircon crystals from rocks of the Kandalaksha massif. Average total amounts of REE in zircon grains typically range from 391.3 ppm to 1815.0 ppm (Table 2). The amount of light REE was minor, which explained the low values of $(Yb/La)_N$ (0.0025–0.0071). These spectra of REE distribution (Figure 5) were characterized by a positive incline with a negative Eu-anomaly and a positive Ce-anomaly, with $(Lu/Gd)_N = 15.05\text{--}18.35$.

Table 2. REE and Ti contents in zircon grains from the metagabbro of the Kandalaksha massif.

Elements	Sample Numbers *		
	183 1-1	183 1-2	183 2-1
	Contents, ppm		
La	1.52	5.43	1.91
Ce	12.6	42.4	53.3
Pr	1.18	6.56	1.01
Nd	14.2	61.3	11.8
Sm	7.57	32.1	11.1
Eu	1.30	6.09	0.32
Gd	17.1	65.1	45.9
Tb	3.95	8.50	15.1
Dy	37.1	65.5	191.3
Ho	16.7	18.0	77.7
Er	79.1	82.1	404.9
Tm	16.6	14.6	88.0
Yb	145.0	160.9	764.1
Lu	37.4	32.0	148.5
Total	391.3	600.5	1815.0

Sample Number	Contents, Ti, ppm	Temperature, °C	T _{aver.} °C
183 1-1	33.8	860.8	
183 2-1 1	36.7	869.7	843.7
183 2-1 2	19.0	800.7	

Note: * average amounts of REE in a crystal.

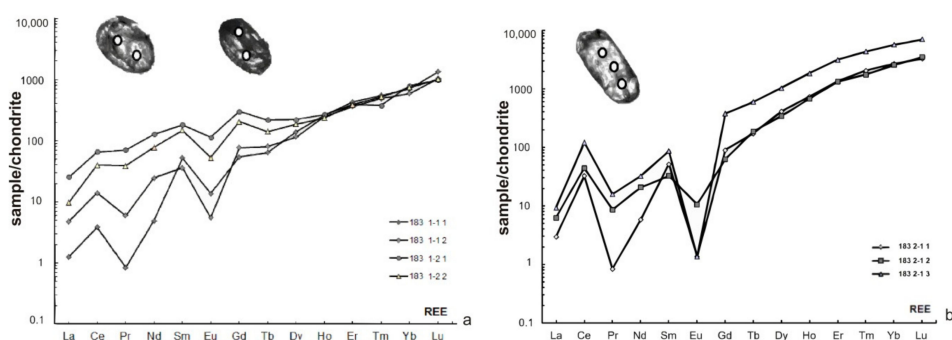


Figure 5. REE pattern in zircons from metagabbro of the Kandalaksha massif (sample 183), normalized after [33]. (a) Samples 183 1-1 and 183 1-2; (b) Sample 183 2-1.

The Ti-in-zircon geothermometer was used to calculate temperatures of zircon grain crystallization [35]. The result indicated an average temperature of 778 ± 44 °C for the zircon grain crystallization in metagabbro.

The average temperature of the U–Pb system closure in measured areas of zircon from metagabbro is 844 °C [35] (Table 2).

4.3. Results of U–Pb and Sm–Nd Dating

The U–Pb analysis on single zircon grains was applied for the first time, using a ^{205}Pb artificial tracer to date zircons from metagabbro of the Kolvitsa massif [36].

The concordant U–Pb age was estimated for both concentrates at 2448 ± 5 Ma (Figure 6a).

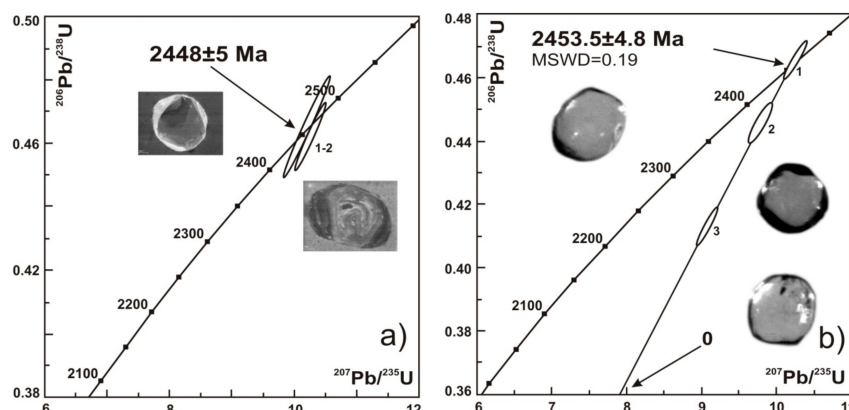


Figure 6. Isotope U–Pb diagrams for single zircon grains from metagabbro of the Kolvitsa (sample 200) (a) and metagabbro of the Kandalaksha (sample 183) (b) massifs.

The new precise U–Pb age on single zircon grains from metagabbro in the Kandalaksha massif yielded to an age of 2453.5 ± 4.8 Ma (Figure 6b, Table 3).

The concordant U–Pb age for single grains of zircon from anorthosites of the Kandalaksha massif (sample 225/1) was estimated for both concentrates at 2230 ± 10 Ma (Figure 7).

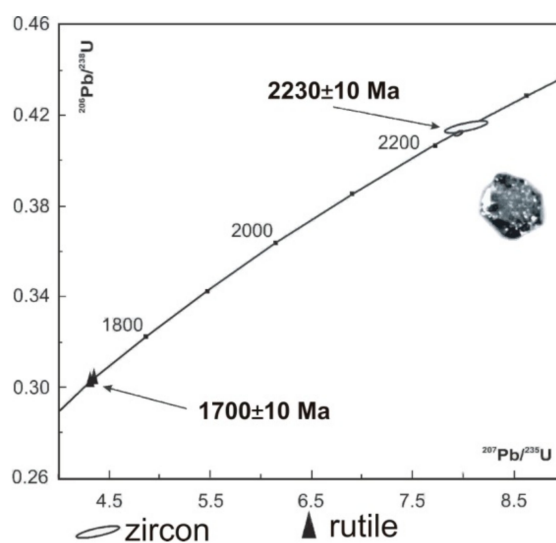


Figure 7. Isotope U–Pb plots for single zircon grains and rutile from anorthosites, Kandalaksha (sample 225/1) massif.

Besides zircon, rutile from anorthosites was dated by the U–Pb method in order to define the age of Svecofennian (1800–1900 Ma) metamorphic events of the amphibolites facies [37,38]. Rutile is represented in the sample by prismatic, semi-transparent, yellowish-brown crystals. The U–Pb age of two weighted portions of rutile was estimated at 1700 ± 10 Ma. It is known that the temperature of the U–Pb system closure for rutile is 400–450 °C [39]. Therefore, the massif cooled down to these temperatures at 1.7 Ga ago. The age of 1.75 Ga is quite common for the Kola Peninsula and relates to fluid processing of rocks at temperatures lower than 450 °C [38].

Table 3. Isotope U–Pb data on single zircon grains from metagabbro and anorthosite, Kandalaksha-Kolvitsa gabbro-anorthosite complex.

Weighted Portion (mg)	Contents, ppm		Isotope Ratios *			Isotope Ratios and Age, Ma **			% Dis.	
	Pb	U	$^{206}\text{Pb}/^{204}\text{Pb}$	$^{206}\text{Pb}/^{238}\text{U}$	$^{207}\text{Pb}/^{235}\text{U}$	$^{207}\text{Pb}/^{206}\text{Pb}$	$^{206}\text{Pb}/^{238}\text{U}$	$^{207}\text{Pb}/^{235}\text{U}$		$^{207}\text{Pb}/^{206}\text{Pb}$
Kolvitsa massif, metagabbro (sample 200), magmatic zircon										
0.0475	11.94	15.97	209.32	0.462 ± 0.008	10.274 ± 0.190	0.1613 ± 0.0006	2448 ± 44	2460 ± 46	2470 ± 8	0.9
0.0800	11.08	15.17	726.92	0.464 ± 0.018	10.225 ± 0.389	0.1644 ± 0.0011	2448 ± 93	2452 ± 93	2461 ± 17	0.5
Kandalaksha massif, metagabbro (sample 183), magmatic zircon										
0.095	46.09	48.60	141.81	0.466 ± 0.006	10.281 ± 0.131	0.1583 ± 0.0005	2468 ± 30	2451 ± 31	2437 ± 8	−1.3
0.200	33.34	24.40	82.01	0.446 ± 0.005	9.798 ± 0.139	0.1595 ± 0.0011	2375 ± 29	2416 ± 34	2451 ± 17	3.1
0.093	74.20	45.76	68.52	0.413 ± 0.005	9.087 ± 0.119	0.1596 ± 0.0006	2228 ± 27	2347 ± 31	2452 ± 10	9.1
Kandalaksha massif, anorthosite (sample 225/1), zircon										
0.200	12.51	13.51	74.95	0.4151 ± 0.0002	8.048 ± 0.0016	0.1406 ± 0.0003	2238 ± 12	2236 ± 47	2235 ± 40	−0.13
0.063	21.08	40.39	781.17	0.4121 ± 0.0002	7.968 ± 0.0024	0.1402 ± 0.0002	2224 ± 10	2227 ± 10	2230 ± 3	0.27

Note: * All ratios are corrected for blanks of 1 pg for Pb and 10 pg for U and for mass discrimination $0.12 \pm 0.04\%$. ** Correction for admixture of common Pb is estimated for the age as per the model described by the authors of [26].

The Sm–Nd dating of metamorphic minerals of gabbro from the Kolvitsa massif (sample 200), anorthosites (sample 225/1), and metagabbro (sample 183) of the Kandalaksha massif was provided, along with the U–Pb geochronological study of accessory minerals. The Sm–Nd analysis estimated the age of metagabbro from the Kolvitsa massif at 1985 ± 17 Ma (Figure 8a), which corresponds with the time of the granulite metamorphism widespread in LGB [40,41]. In general, using sulfides as geochronometers provides positive results for a number of commercially valued objects of the Baltic Shield [42].

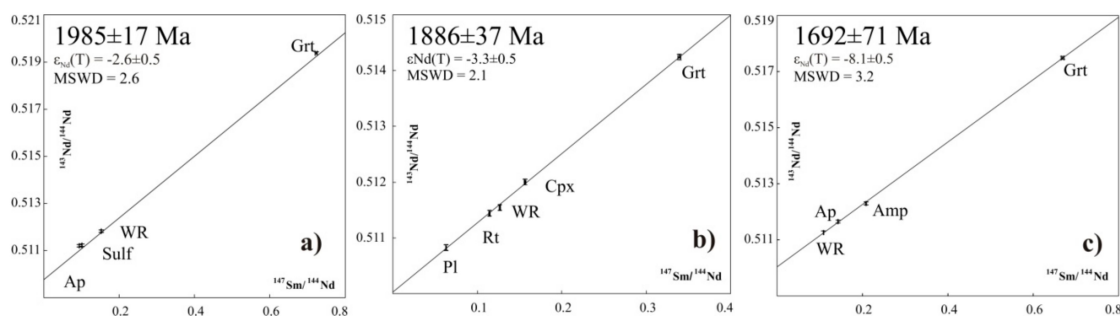


Figure 8. Isotope Sm–Nd isochrones for metamorphic minerals from metagabbroids of the Kolvitsa massif (sample 200) (a), rock-forming and metamorphic minerals from anorthosites (sample 225/1) (b), and gabbro (sample 183) (c) of the Kandalaksha massif.

The model Sm–Nd age of these gabbroids was close to 3.3 Ga (Table 4), which is typical of the Paleoproterozoic ore-magmatic system of the Baltic Shield [43].

Table 4. Results of the Sm–Nd isotope analysis of rocks and minerals from the Kolvitsa and Kandalaksha gabbro-anorthosite complexes.

Sample	Contents, mkg/g		Isotope Ratios		T_{DM} , Ma
	Sm	Nd	$^{147}\text{Sm}/^{144}\text{Nd}$	$^{143}\text{Nd}/^{144}\text{Nd}$	
Sample 225/1, anorthosite, Kandalaksha massif					
225/1 WR	0.419	2.00	0.1265	0.511544 ± 8	2796
225/1 Pl	0.181	1.743	0.0627	0.510823 ± 34	
225/1 Ru	0.399	2.11	0.1143	0.511440 ± 24	
225/1 Cpx	2.40	9.26	0.1564	0.512000 ± 7	
225/1 Gr	0.513	0.915	0.3392	0.514235 ± 20	
Sample 183, metagabbro, Kandalaksha massif					
183 WR	0.459	2.553	0.1087	0.511263 ± 31	2728
183 Ap	20.1	85.2	0.1427	0.511653 ± 15	
183 Amf	2.39	6.93	0.2084	0.512290 ± 8	
183 Gr-3	1.252	1.131	0.6689	0.517489 ± 17	
Sample 200, metagabbro, Kolvitsa massif					
200 WR	0.845	3.35	0.1524	0.511823 ± 9	3300
200 Sulf	0.068	0.435	0.0940	0.511204 ± 23	
200 Ap	23.5	140.4	0.1011	0.511226 ± 12	
200 Gr	0.660	0.552	0.7234	0.519387 ± 17	

Note: WR—whole rock, Ap—apatite, Amp—amphibole, Cpx—clinopyroxene, Gr—garnet, P—plagioclase, Ru—rutile, Sulf—sulfide minerals. The mean value of the $^{143}\text{Nd}/^{144}\text{Nd}$ in the La Jolla standard for the test period was 0.511835 ± 18 (N = 15).

Rutile, garnet, plagioclase, clinopyroxene, and whole rocks from metaanorthosites of the Kandalaksha massif (sample 225/1) displayed the age of 1886 ± 37 Ma on the Sm–Nd plot in isochron coordinates (Figure 8b, Table 4). Conditions of the granulite facies typically had temperatures of about 900–800 °C. Thus, it can be assumed that the Sm–Nd systems were transformed. The close Sm–Nd age (1886 ± 9 Ma) was obtained for sillimanite-orthopyroxene-garnet rocks of the Porya Guba cover of LGB. It is interpreted by the authors of [44] as the age of the high-temperature metasomatism.

The Sm–Nd age of metamorphosed leucogabbro in the Kandalaksha massif (sample 183) was estimated on the whole rock, apatite, amphibole, and garnet at 1692 ± 71 Ma (Figure 8c, Table 4). It is close to the U–Pb age of rutile and seems to mark the processes of cooling or low-temperature processing in the rocks of the Kandalaksha massif at the edge of 1.7 Ga. Check tests on mixing in coordinates $1/[Nd]—^{143}Nd/^{144}Nd$ for all of the studied rocks showed no correlation between Nd contents and isotope compositions. Thus, the obtained age can be interpreted as the age of the geological event (metasomatism) despite the increased MSWD. The age of 1.7 Ga is quite common for the Kola Peninsula and can be related to fluid processing of rocks at temperatures lower than 450 °C [38].

4.4. Geochemical Nd–Sr Data

In addition, isotope compositions of Sr were analyzed to draw a plot in coordinates $\epsilon_{Nd}(T)$ – I_{Sr} (Figure 9, Table 5).

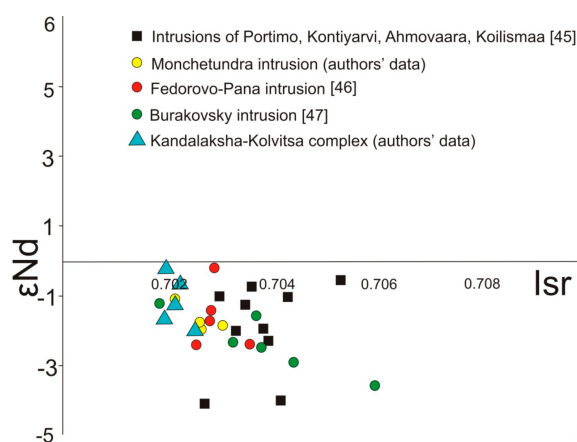


Figure 9. Variations of ϵ_{Nd} and I_{Sr} in rocks of layered Proterozoic intrusions in the Baltic Shield [45–47].

Table 5. Results of the Nd–Sr isotope analysis of rocks from the Kolvitsa and Kandalaksha massifs.

Contents, mkg/g		Isotope Ratios		T, Ma	Isr	Contents, mkg/g		Isotope Ratios		T _{DM} , Ma	$\epsilon_{Nd}(T)$	Age, Ga
Rb	Sr	$^{87}Rb/^{86}Sr$	$^{87}Sr/^{86}Sr$			Sm	Nd	$^{147}Sm/^{144}Nd$	$^{143}Nd/^{144}Nd$			
Sample 220/1, metanorite, Kandalaksha massif												
16.49	259.0	0.1796	0.70744 ± 18	2100	0.7020	0.155	0.916	0.1025	0.511116 ± 31	2776	−0.02	
Sample 225/1, anorthosite, Kandalaksha massif												
						0.419	2.003	0.1265	0.511544 ± 8	2796	−1.23	1.9
Sample 183, metagabbro, Kandalaksha massif												
7.37	367.3	0.0566	0.70426 ± 16	2453	0.7023	0.459	2.553	0.1087	0.511263 ± 31	2728	−1.25	1.7
Sample 185, metaperidotite, Kandalaksha massif												
13.73	90.6	0.4277	0.71758 ± 17	2450	0.7024	1.407	6.489	0.131015	0.511532 ± 7	2969	−0.95	
Sample 200, metagabbro, Kolvitsa massif												
6.59	249.6	0.0745	0.70516 ± 12	2448	0.7025	0.845	3.354	0.1524	0.511823 ± 9	3282	−1.96	1.9
Sample 205, subalkaline gneiss-granite, Kolvitsa massif												
89.12	114.9	2.1884	0.78443 ± 18	2383	0.7091							
Sample 194/1, metagabbro, Kolvitsa massif												
2.78	427.0	0.0184	0.70221 ± 15	2450	0.7016							
Sample 210, gneiss-plagiogranite, TTG-?, Kolvitsa massif												
60.93	235.7	0.729350	0.72950 ± 19	2450	0.70193	2.007	10.835	0.111983	0.511192 ± 9	2920	−1.59	
Sample 276, garnet-plagioclase crystal schist, Kolvitsa massif												
10.42	211.55	0.138969	0.70742 ± 14			6.891	20.935	0.198946	0.512396 ± 9		−5.53	

5. Discussion

The obtained data on the REE content and pattern in the zircon of the Kandalaksha and Kolvitsa massifs is typical for zircon with the magmatic origin [34]. The average temperature of the U–Pb

system closure and zircon grain crystallization (according to [35]) in measured areas of zircon from metagabbro Kandalaksha massif is 844 °C. Zircon grain crystallization occurs in metagabbro of the Kolvitsa massif at the average temperature of 778 °C. The studied zircon was likely to have formed at the late stage of the Kolvitsa massif crystallization. The obtained data on temperatures of zircon crystallization and closure of the U–Pb system are typical of magmatic zircons and correspond with the previously obtained data on zircons from gabbro-anorthosite complexes in North America [48].

The estimated U–Pb age (2448 ± 5 Ma) of metagabbro from the Kolvitsa massif is considered magmatic due to low contents of U and Pb typical of magmatic zircons from basic rocks and spectra of REE distribution. The obtained U–Pb age is interpreted as the time of gabbro formation in the Kolvitsa massif [13] and is close to previously calculated ages of anorthosites from this massif [7,8].

The new precise U–Pb age on single zircon grains (2453.5 ± 4.8 Ma) is interpreted as the time of the magmatic formation of metagabbro in the Kandalaksha massif. Both zircon types showed concordant U–Pb ages of 2230 ± 10 Ma considering errors in estimations. This age reflects the early stage of the granulite metamorphism superimposed on anorthosites of the Kandalaksha massif.

According to geochronological and Nd–Sr isotope data, rocks of the Kandalaksha-Kolvitsa complex seemed to have a common anomalous mantle source with Paleoproterozoic layered intrusions of the Baltic Shield (Figure 9). The obtained data comply with the known isotope-geochemical characteristics of ore-bearing layered intrusions in the northeastern Baltic Shield [40,43,46]. The model age of rocks from the Kandalaksha-Kolvitsa complex varied from 2.8 Ga to 3.3 Ga and corresponded with T_{DM} for rocks in the East-Scandinavian Large Igneous Province [46]. Rocks of these intrusions that belong to the pyroxenite-gabbronorite-anorthosite formation had similar isotope-geochemical features, as follows:

- The age range of the formation was 2530 Ma to 2400 Ma, according to U–Pb and Sm–Nd geochronological data;
- The mantle reservoir, which is a source of the magmas that produced the massifs, was rich in lithophile elements. I_{Sr} values varied from 0.702 to 0.706, $\epsilon_{Nd}(T)$ values varied from -0.02 to -3 , and model Sm–Nd ages of the T_{DM} protoliths were 2.8–3.3 Ga.

6. Conclusions

New U–Pb and Sm–Nd isotope data on massifs of the Kandalaksha-Kolvitsa gabbro-anorthosite complex suggested the following sequence of geological events. Gabbro-anorthosite massifs were crystallized at 2448 ± 5 Ma, at the same time as the most extensive intracontinental rifting in the region. The further evolution of the massifs is related to their long-term structural-metamorphic processing that lasted for 250 Ma. During this processing, the massifs were subjected to the granulite metamorphism of two stages, i.e., the early one at 2230 ± 10 Ma, and the later one at 1985 ± 17 Ma. High-temperature metasomatic changes of the massifs occurred at 1887 ± 37 Ma. The final cooling of the massifs to the temperature of 400–450°C happened at 1692 ± 71 Ma– 1700 ± 10 Ma and was associated with fluid processing. Results of complex isotope-geochemical, geochronological, petrological-mineralogical research suggest that the mantle source with anomalous isotope characteristics is the common source of the matter in the Paleoproterozoic layered complexes in Fennoscandia. Geochronological and Nd–Sr isotope data indicated that rocks of the Kandalaksha-Kolvitsa complex could have a common anomalous mantle source with Paleoproterozoic layered intrusions in the Baltic Shield (T_{DM} —2.8–3.3 Ga, I_{Sr} varies from 0.702 to 0.706, $\epsilon_{Nd}(T)$ varies from -0.02 to -3).

Author Contributions: Conceptualization, E.N.S.; Methodology, E.N.S., T.B.B., and P.A.S.; Validation, E.N.S., T.B.B., and P.A.S.; Formal Analysis, P.A.S.; Investigation, E.N.S., T.B.B., P.A.S.; Data Curation, T.B.B. and P.A.S.; Writing—Original Draft Preparation, E.N.S.; Writing—Review and Editing, E.N.S.; Visualization, E.N.S., T.B.B., and P.A.S.; Supervision, E.N.S. All authors have read and agreed to the published version of the manuscript.

Funding: This research was funded by the Scientific Research Contract of GI KSC RAS No. 0226-2019-0053, grants of the Russian Foundation for Basic Research No. 18-05-70082 «Arctic Resources», 18-35-00246 mol_a, and the Presidium RAS Program No. 8.

Conflicts of Interest: The authors declare no conflict of interest.

References

1. Polat, A.; Appel, P.W.U.; Fryer, B.; Windley, B.; Frei, R.; Samson, I.M.; Huang, H. Trace element systematics of the Neoproterozoic Fiskensæset anorthosite complex and associated meta-volcanic rocks, SW Greenland: Evidence for a magmatic arc origin. *Precambrian Res.* **2009**, *175*, 87–115. [CrossRef]
2. Polat, A.; Fryer, B.J.; Appel, P.W.U.; Kalvig, P.; Kerrich, R.; Dilek, Y.; Yang, Z. Geochemistry of anorthositic differentiated sills in the Archean (~2970Ma) Fiskensæset Complex, SW Greenland: Implications for parental magma compositions, geodynamic setting, and secular heat flow in arcs. *Lithos* **2011**, *123*, 50–72. [CrossRef]
3. Hoffmann, J.E.; Svahnberg, H.; Piazzolo, S.; Scherstén, A.; Münker, C. The geodynamic evolution of Mesoproterozoic anorthosite complexes inferred from the Naajat Kuuat Complex, southern West Greenland. *Precambrian Res.* **2012**, *196–197*, 149–170. [CrossRef]
4. Mitrofanov, F.P. Prospecting indicators for new industrial deposits of Ro–Pt–Pd and Co–Cu–Ni and Cr ores on the Kola Peninsula. *Otechestvennaya Geol.* **2006**, *4*, 3–9. (In Russian)
5. Mitrofanov, F.P. *Geological Map of the Kola region. Scale 1:500000*; GIS ArcView 3.0; Regional Geophysics Lab., GI KSC RAS: Apatity, Russia, 1996; Available online: <http://www.geokniga.org/maps/5457> (accessed on 9 March 2020).
6. Mitrofanov, F.P.; Bayanova, T.B.; Korchagin, A.U.; Groshev, N.Y.; Malitch, K.N.; Zhironov, D.V.; Mitrofanov, A.F. East Scandinavian and noril'sk plume mafic large igneous provinces of Pd–Pt ores: Geological and metallogenic comparison. *Geol. Ore Depos.* **2013**, *55*, 305–319. [CrossRef]
7. Mitrofanov, F.P.; Balagansky, V.V.; Balashov, Y.A.; Gannibal, L.F.; Dokuchaeva, V.S.; Nerovich, L.I.; Radchenko, M.K.; Rünginen, G.I. U–Pb age of gabbro-anorthosites of the Kola Peninsula. *Dokl. Akad. Nauk* **1993**, *331*, 1. (In Russian)
8. Frisch, T.; Jackson, H.; Glebovitsky, V.A.; Efimov, M.M.; Bogdanova, M.N.; Parrish, P.P. U–Pb geochronology of zircon of the Kolvitsa gabbro-anorthosite complex, southern part of the Kola Peninsula, Russia. *Petrologiya* **1995**, *3*, 248–254. (In Russian)
9. *The Early Precambrian of the Baltic Shield*; Glebovitsky, V.A. (Ed.) Nauka: St. Petersburg, Russia, 2005; p. 711. (In Russian)
10. Balagansky, V.V.; Timmerman, M.Y.; Kislitsyn, R.V.; Daily, J.S.; Balashov, Y.A.; Gannibal, L.F.; Sherstennikova, O.G.; Rünginen, G.I. Isotope age of rocks of the Kolvitsa belt and Umba block (south-eastern flank of the Lapland Granulite Belt), Kola Peninsula. *Vest. MSTU* **1998**, *1*, 19–32. (In Russian)
11. Nikolaev, A.I.; Drogobuzhskaya, S.V.; Bayanova, T.B.; Kaulina, T.V.; Lyalina, L.M.; Novikov, A.I.; Steshenko, E.N. REE distribution in zircon from reference rocks of the Arctic region: evidence from study by the LA-ICP-MS method. *Doklady Earth Sci.* **2016**, *470*, 1037–1041. [CrossRef]
12. Steshenko, E.N.; Nikolaev, A.I.; Bayanova, T.B.; Drogobuzhskaya, S.V.; Chashchin, V.V.; Serov, P.A.; Lyalina, L.M.; Novikov, A.I. The Paleoproterozoic Kandalaksha anorthosite massif: New U–Pb (ID-TIMS) data and geochemical features of zircon. *Doklady Earth Sci.* **2017**, *477*, 1454–1457. [CrossRef]
13. Steshenko, E.N.; Nikolaev, A.I.; Bayanova, T.B.; Drogobuzhskaya, S.V.; Chashchin, V.V.; Serov, P.A.; Lyalina, L.M.; Novikov, A.I.; Elizarov, D.V. The Paleoproterozoic Kolva anorthosite block: New data on the U–Pb age (ID-TIMS) and geochemical features of zircon. *Doklady Earth Sci.* **2018**, *479*, 366–370. [CrossRef]
14. Certificate of Analysis. Standard Reference Material 612. In *Trace Element in Glass*; NIST: Gaithersburg, MD, USA, 2012; pp. 1–4.
15. Pearce, N.J.G.; Perkins, W.T.; Westgate, J.A. A compilation of new and published major and trace element data for NIST SRM 610 and NIST SRM 612 glass reference materials. *Geostand. Newslett.* **1997**, *21*, 115–144. [CrossRef]
16. Jochum, K.P.; Weis, U.; Stoll, B.; Kuzmin, D.; Yang, Q.; Raczek, I.; Jacob, D.E.; Stracke, A.; Birbaum, K.; Frick, D.A.; et al. Determination of reference values for NIST SRM 610–617 Glasses Following ISO Guidelines. *Geostand. Geoanal. Res.* **2011**, *35*, 397–429. [CrossRef]
17. Reischmann, T.; Brugmann, G.E.; Jochum, K.P.; Todt, W.A. Trace element and isotopic composition of baddeleyite. *Miner. Petrol.* **1995**, *53*, 155–164. [CrossRef]
18. Schmitt, A.K.; Chamberlain, K.R.; Swapp, S.M.; Harrison, T.M. In situ U–Pb dating of micro-baddeleyite by secondary ion mass spectrometry. *Chem. Geol.* **2010**, *269*, 386–395. [CrossRef]

19. Li, Q.L.; Li, X.H.; Liu, Y.; Tang, G.Q.; Yanga, J.H.; Zhu, W.G. Precise U–Pb and Pb–Pb dating of Phanerozoic baddeleyite by SIMS with oxygen flooding technique. *J. Anal. At. Spectrom.* **2010**, *25*, 1107–1113. [[CrossRef](#)]
20. Krogh, T.E. A low-contamination method for hydrothermal dissolution of zircon and extraction of U and Pb for isotopic age determinations. *Geochim. Cosmochim. Acta* **1973**, *37*, 485–494. [[CrossRef](#)]
21. Schärer, U.; Gower, C.F. Crustal evolution in Eastern Labrador: Constraints from precise U–Pb ages. *Precambrian Res.* **1988**, *38*, 405–421. [[CrossRef](#)]
22. Schärer, U.; Wilmart, E.; Duchesne, J.C. The short duration and anorogenic character of anorthosite magmatism: U–Pb dating of the Rogaland Complex, Norway. *Earth Planet. Sci. Lett.* **1996**, *139*, 335–350. [[CrossRef](#)]
23. Ludwig, K.R. *PB DAT: A Computer Program for Processing Pb–U–Th Isotope Data, Version 1.22*; Open-File Report 88-542; United States Geological Survey: Reston, VA, USA, 1991; 33p.
24. Ludwig, K.R. *ISOPLOT/Ex: A Geochronological Toolkit for Microsoft Excel, Version 2.05*; Berkeley Geochronology Center Special Publication: Berkeley, CA, USA, 1999; Volume 1, p. 49.
25. Steiger, R.; Jäger, E. Subcommittee on geochronology: Convention on the use of decay constants in geo- and cosmochronology. *Earth Planet. Sci. Lett.* **1977**, *36*, 359–362. [[CrossRef](#)]
26. Stacey, J.S.; Kramers, J.D. Approximation of terrestrial lead isotope evolution by a two-stage model. *Earth Planet. Sci. Lett.* **1975**, *26*, 207–221. [[CrossRef](#)]
27. Raczek, I.; Jochum, K.P.; Hofmann, A.W. Neodymium and strontium isotope data for USGS reference materials BCR-1, BCR-2, BHVO-1, BHVO-2, AGV-1, AGV-2, GSP-1, GSP-2 and eight MPI-DING reference glasses. *Geostand. Geoanalytical Res.* **2003**, *27*, 173–179. [[CrossRef](#)]
28. Tanaka, T.; Togashi, S.; Kamioka, H.; Amakawa, H.; Kagami, H.; Hamamoto, T.; Yuhara, M.; Orihashi, Y.; Yoneda, S.; Shimizu, H.; et al. JNdi-1: A neodymium isotopic reference in consistency with LaJolla neodymium. *Chem. Geol.* **2000**, *168*, 279–281. [[CrossRef](#)]
29. Ludwig, K.R. ISOPLOT/Ex—A geochronological toolkit for Microsoft Excel, Version 3.6. *Berkeley Geochronol. Cent. Spec. Publ.* **2008**, *4*, 76.
30. Bouvier, A.; Vervoort, J.D.; Patchett, P.J. The Lu–Hf and Sm–Nd isotopic composition of CHUR: Constraints from unequilibrated chondrites and implications for the bulk composition of terrestrial planets. *Earth Plan. Sci. Lett.* **2008**, *273*, 48–57. [[CrossRef](#)]
31. Goldstein, S.J.; Jacobsen, S.B. Nd and Sr isotopic systematics of river water suspended material implications for crystal evolution. *Earth Plan. Sci. Lett.* **1988**, *87*, 249–265. [[CrossRef](#)]
32. Weis, D.; Kieffer, B.; Maerschalk, C.; Barling, J.; De Jong, J.; Williams, G.A.; Hanano, D.; Pretorius, W.; Mattioli, N.; Scoates, J.S.; et al. High-precision isotopic characterization of USGS reference materials by TIMS and MC-ICP-MS. *Geochem. Geophys. Geosystems* **2006**, *7*, Q08006. [[CrossRef](#)]
33. Boynton, W.V. Cosmochemistry of the rare earth elements: Meteorite studies. In *Developments in Geochemistry*; Henserson, P., Ed.; Elsevier: Amsterdam, the Netherlands, 1984; pp. 63–114.
34. Hoskin, P.W.O.; Schaltegger, U. The composition of zircon and igneous and metamorphic petrogenesis. *Rev. Mineral. Geochem.* **2003**, *53*, 27–62. [[CrossRef](#)]
35. Watson, E.B.; Wark, D.A.; Thomas, J.B. Crystallization thermometers for zircon and rutile. *Contrib. Mineral. Petrol.* **2006**, *151*, 413–433. [[CrossRef](#)]
36. Bayanova, T.B.; Corfu, F.; Todt, V.; Poller, U.; Levkovich, N.; Apanasevich, E.; Zhavkov, V. Heterogeneity of the 91500 and TEMORA-1 Standards for U–Pb Dating of Single Zircons. In Proceedings of the XVIII Symposium on Geochemistry of Isotopes dedicated to Acad, Moscow, Russia, 14–16 November 2007; pp. 42–43. (In Russian)
37. Bibikova, E.V.; Bogdanova, S.V.; Glebovitsky, V.A.; Klaisson, S.; Sheld, T. Stages of the White Sea mobile belt evolution according to the data of U–Pb zircon geochronology (ion microprobe analyzer NORDSIM). *Petrologiya* **2004**, *12*, 227–244. (In Russian)
38. Kaulina, T.V. *Formation and Transformation of Zircon in Polymetamorphic Complexes*; Kola Science Centre RAS: Apatity, Russia, 2010; p. 144. (In Russian)
39. Mezger, K.; Hanson, G.N.; Bohlen, S.R. High-precision U–Pb ages of metamorphic rutile: application to the cooling history of high-grade terrains. *Earth Plan. Sci. Lett.* **1989**, *96*, 106–118. [[CrossRef](#)]
40. Bayanova, T.B. *The Age of Reference Geological Complexes of the Kola Region and Duration of Magmatism Processes*; Nauka: St. Petersburg, Russia, 2004; p. 174. (In Russian)

41. Pozhilenko, V.I.; Gavrilenko, B.V.; Zhirov, D.V.; Zhabin, S.V. *Geology of Ore Areas of the Murmansk Region*; Kola Science Centre RAS: Apatity, Russia, 2002; p. 359. (In Russian)
42. Serov, P.A. *Age Frontiers of the PGE Occurrence Formation in the Fedorovo-Pana Layered Massif, according to Sm–Nd and Rb–Sr Isotope Characteristics*; Cand. Sci. (Geol.-mineral.) Thesis; AutoAbstr: Voronezh, Russia, 2008; p. 20. (In Russian)
43. Bayanova, T.; Korchagin, A.; Mitrofanov, A.; Serov, P.; Ekimova, N.; Nitkina, E.; Kamensky, I.; Elizarov, D.; Huber, M. Long-lived mantle plume and polyphase evolution of Palaeoproterozoic PGE intrusions in the Fennoscandian Shield. *Minerals* **2019**, *9*, 59. [[CrossRef](#)]
44. Lebedeva, Y.M.; Glebovitsky, V.A.; Bushmin, S.A.; Bogomolov, E.S.; Savva, E.V.; Lokhov, K.I. The age of high-bar metasomatism in shift areas under the collision metasomatism in the Lapland Granulite Belt: Sm–Nd method of dating parageneses from sillimanite-orthopyroxene rocks of the Porya Guba cover. *Doklady Akad. Nauk* **2010**, *432*, 99–102. (In Russian)
45. Huh, H.; Cliff, R.; Perttunen, V.; Sakko, M. Sm–Nd and Pb isotopic study of mafic rocks associated with early Proterozoic continental rifting: The Perapohja schist belt in northern Finland. *Contrib. Mineral. Petrol.* **1990**, *104*, 369–379. [[CrossRef](#)]
46. Mitrofanov, F.P.; Bayanova, T.B.; Ludden, J.N.; Korchagin, A.U.; Chashchin, V.V.; Nerovich, L.I.; Serov, P.A.; Mitrofanov, A.F.; Zhirov, D.V. Origin and Exploration of the Kola PGE-bearing Province: New Constraints from Geochronology. In *Ore Deposits: Origin, Exploration, and Exploitation*; Decree, S., Robb, L., Eds.; Wiley: Hoboken, NJ, USA, 2019; pp. 3–36.
47. Amelin, Y.V.; Semenov, V.S. U–Nd and Sr isotopic geochemistry of mafic layered intrusions in the eastern Baltic Shield: implications for the evolution of Paleoproterozoic continental mafic magmas. *Contrib. Miner. Petrol.* **1996**, *124*, 255–272. [[CrossRef](#)]
48. Fu, B.; Page, F.Z.; Cavosie, A.J.; Fournelle, J.; Kita, N.T.; Lackey, J.S.; Wilde, S.A.; Valley, J.W. Ti-in-zircon thermometry: Applications and limitations. *Contrib. Mineral. Petrol.* **2008**, *156*, 197–215. [[CrossRef](#)]



© 2020 by the authors. Licensee MDPI, Basel, Switzerland. This article is an open access article distributed under the terms and conditions of the Creative Commons Attribution (CC BY) license (<http://creativecommons.org/licenses/by/4.0/>).